Marine Geology 448 (2022) 106812

Contents lists available at ScienceDirect

Marine Geology

journal homepage: www.elsevier.com/locate/margo

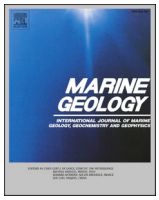

Research Article

A mechanism for high-frequency variability in sapropels

J.P. Dirksen *, P. Meijer

Department of Earth Sciences, Utrecht University, Utrecht, the Netherlands

ARTICLE INFO

Editor: Dr. Shu Gao

Keywords:
Sapropels
Transient box model
High-frequency variability

ABSTRACT

Sapropels deposited in the Mediterranean Sea provide high resolution records of past oceanographic changes. Previous studies have found abrupt transitions in chemical composition of these sediments. We present a transient box model that provides a potential mechanism for these transitions. The high-frequency variability is a result of fluxes stopping or changing direction, causing a relaxation towards a new equilibrium. The time scales depend on the volume of the reservoirs and the magnitude of the fluxes. We find typical periods in the order of 100–1000 years, similar to what has been found in sediment cores.

1. Introduction

Rapid changes as a result of a comparatively low-frequency forcing are of interest as they provide new insight into mechanisms that could affect climate change on human time scales. Here we study high-frequency variability in the Mediterranean Sea with a new transient box model. Previous studies on high-frequency variability mostly focused on high latitudes. The ice sheets are known to show significant variability on the Milankovitch time scales as well as on centennial to millennial time scales. They provide very high temporal resolution and also sufficient length to capture long term variability, up to 2.7 Myrs (Bibby et al., 2016). Therefore, these records are ideal to study the impact of relatively slow variations on variability that occurs much faster. For example, relatively slow Heinrich events have been hypothesized to excite the faster Dansgaard–Oeschger cycles (Sampieri, 2002; Timmermann et al., 2003). In turn, Heinrich events are linked to much slower glacial-interglacial cycles which are forced by orbital variability, mainly on 100 *kyr* time scales (Timmermann et al., 2003). Another mechanism linking high and low-frequency variability is described in Starr et al. (2020): icebergs traveling further north from the Southern Ocean into the South Atlantic play a key role in the onset of the ice ages. This can only occur when sufficient cooling has already happened, typically due to Milankovitch variability. So, in this case, the low-frequency variability is a boundary condition for the fast variability, which in turn triggers low-frequency variability. At low latitudes, records of sufficient resolution and length to detect the interaction of Milankovitch and higher frequency variability are rare. Most records either lack the resolution due to bioturbation, insufficient sampling, or poor time control, or are limited to the last few thousand years (for example Mercone et al., 2001; Incarbona et al., 2011; Llave et al., 2006).

The geological record of the Eastern Mediterranean Sea contains regularly occurring organic-rich layers, called sapropels. The deposition of these layers coincides with increased Nile outflow due to enhanced African summer monsoon activity during precession minima (Rossignol-Strick, 1985; Rohling et al., 2015). This additional freshwater is hypothesized to form a lid on the Mediterranean Sea, slowing down or even stopping the circulation. The lack of circulation in turn stops bottom water ventilation, preserving organic matter and preventing bioturbation. Sapropels thus provide a high resolution record of changes in thermohaline circulation. Dirksen et al. (2019) observed such variability on multicentennial time scales in sapropel S5 in a core from the Levantine basin. Sierro et al. (2020) studied the sedimentary record of the Mediterranean outflow on the Atlantic side of the Gibraltar strait using sediment core data, linking changes in outflow velocity to the millennial scale variability of the Greenland ice sheet.

In this study we use a so-called box model. A box represents a homogeneous water mass, which interacts with the surrounding boxes. The interaction represents physical processes, such as convection and strait transport. Rather than calculating the water properties and circulation that are in equilibrium with a changed forcing (e.g., an insolation maximum), we use the model to follow the system as a function of time (for an entire precession cycle), doing justice to its transient nature. We represent the Mediterranean Sea by five dynamic water boxes. The boundary conditions are represented by additional boxes that have constant or predetermined properties. In Dirksen and Meijer (2020) we showed that a box model can capture the primary features of sapropel

* Corresponding author.
E-mail address: pieter.dirksen@live.nl (J.P. Dirksen).

https://doi.org/10.1016/j.margeo.2022.106812
Received 24 December 2021; Received in revised form 14 April 2022; Accepted 25 April 2022
Available online 28 April 2022

formation and give insight into timing and other fundamental mechanisms. This model, however, does not capture some of the high-frequency variability observed in proxy records (e.g. in sapropel S5, Dirksen et al., 2019). The extended model, with additional intermediate water boxes, presented here allows for more complex behaviour and can therefore be used to improve our understanding of processes that act on shorter time scales. We find that when a flux stops or reverses, the equilibrium state of most system variables changes significantly. This causes a fast transition towards the new dynamic equilibrium. This high-frequency variability is independent of the forcing frequency. The time scales are entirely dependent on the dynamics and sizes of the volumes concerned. Since the model has multiple boxes many transitions can occur in one run. The results imply that when interpreting high resolution proxy records, one should always be mindful that a significant part of the variability may be caused by non-linear internal processes instead of external forcing. For example, when fluxes change direction, a given water mass suddenly receives water from a different source, with different properties. That could cause a jump in, for example, temperature. When such a jump in temperature is observed in a geological record, one may erroneously conclude that very rapid climate change occurred. These principles apply to all records of past oceanographic and climatic variability. For sapropels in the Mediterranean Sea this implies that interruptions, sudden terminations and internal variability may largely be caused by the non-linear response of the ocean to much slower forcing.

2. Methods

To be able to study the more complex behaviour found in sediment cores, we introduce separate surface and intermediate boxes, while retaining the model framework of Dirksen and Meijer (2020). The main components of the extended model are explained here. A complete description of all model equations and details about the way these are combined and solved, can be found Dirksen and Meijer (2020) in combination with the annotated model code (see link to public repository near end of paper). Throughout this paper, we use Matlab as our computational environment. The layout of the model is shown in Fig. 1. As in our previous paper we set out to capture the essence of the Mediterranean Sea and consider a single main basin (open basin) connected to the Atlantic Ocean and having a single marginal sub basin. This allows us to focus on the primary effects of having a separate intermediate water layer. The properties of the Atlantic box are kept constant and the model is forced at the surface by prescribing the flux of freshwater (evaporation, precipitation and river discharge) and an atmospheric temperature to which the temperature of each surface box is relaxed. The present-day Mediterranean Sea has a small annual heat loss (Song and Yu, 2017). The model captures this by assuming perpetual winter conditions for the atmosphere, following Dirksen and Meijer (2020). As a consequence, the Atlantic box is always the water box with the highest temperature in the model. Forcings are defined separately for the open and the marginal box. Given these boundary conditions, the model uses conservation of water, salt and heat to solve for the salinity and temperature of the five Mediterranean boxes and for the magnitude of the water fluxes between the various parts.

While some of the fluxes are “compensating” (Fig. 1) in that their value at any given point in time follows from the requirement to conserve volume, others are determined by the density difference between the interacting boxes. Density is calculated from salinity and temperature using the EOS80 formula (on Oceanographic Tables, 1986).

In both straits comprised by the model, the deeper of the two fluxes is considered density-driven. That is, horizontal flux at intermediate depth is from the box with higher density towards that with lower density. The flux is made proportional to the square root of the density difference, as would be appropriate for a hydraulically-controlled strait exchange (e.g. Meijer, 2021). The factor of proportionality is termed the coefficient of strait efficiency and its value is chosen a priori. If a strait accommodates intermediate-depth inflow into the open basin and the density of the water it carries exceeds that of the deep water, the flux will sink into the deep-water box. Also with reference to the vertical direction, convection is taken to occur when the density of the overlying box exceeds the density of the lower box. Convection consists of two fluxes that always flow in both directions simultaneously. In the model, the magnitude of

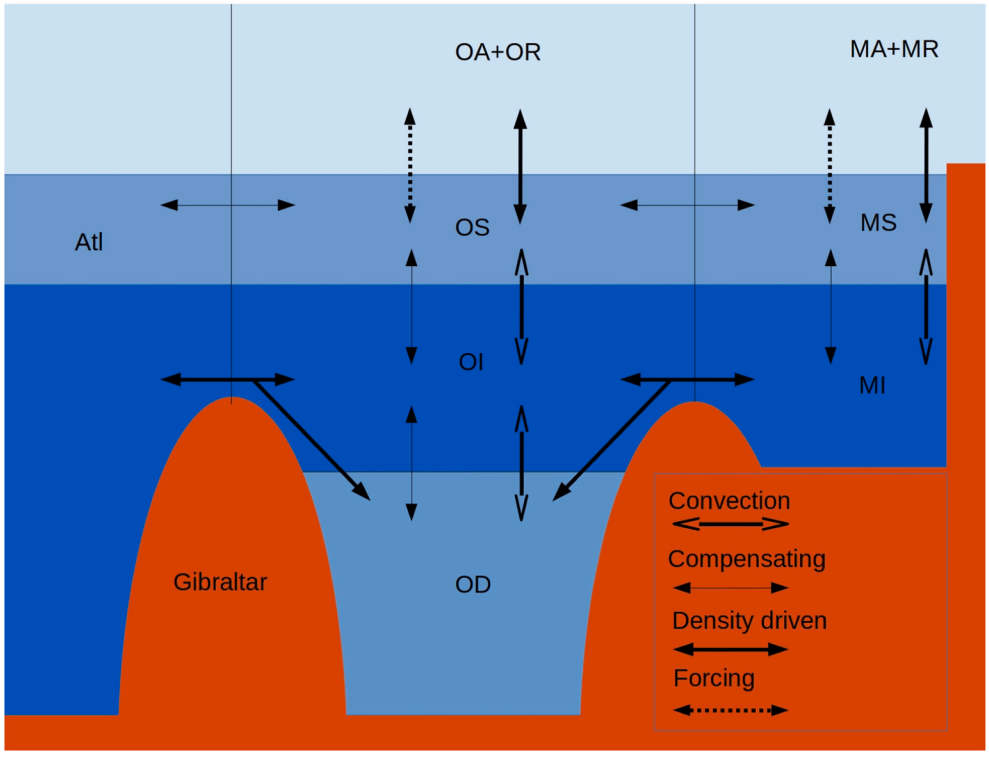

Fig. 1. A schematic representation of the model, showing the Atlantic (Atl), Open Atmosphere (OA) and Open River (OR), Open Surface (OS), Open Intermediate (OI), Open Deep (OD), Marginal Atmosphere (MA), Marginal River (MR), Marginal Surface (MS) and Marginal Intermediate boxes are indicated. The margin represents the Aegean Sea and the Adriatic Sea and the Open basin represents Western basin, Eastern Basin, Levantine Sea and the Gulf of Lion (see Fig. 6). The convection fluxes also include diffusive mixing. The “density driven” exchange with the atmosphere represents temperature relaxation. The forcing ecompasses both evaporation and river discharge.

these fluxes is linearly dependent on the density difference. Diffusive mixing is included as a constant "flux" in the same formula. The total exchange in one time step is limited to the volume of the smallest box involved, to prevent unrealistic behaviour.

The forcing function is a 20 *kyr* sine wave, representing climatic precession. This sine wave modulates river outflow and net evaporation (i.e. the difference between evaporation and precipitation) with realistic values. The other parameters, such as atmospheric temperature, are kept constant. The freshwater budgets of the surface boxes is made to change sign for part of the cycle (similar to Dirksen and Meijer, 2020). Although there is no evidence that the intermediate water flow at Gibraltar or Sicily changed direction, even during the most extreme anoxic events (Zahn et al., 1987; Rogerson et al., 2005; Schönfeld, 2002; Schönfeld and Zahn, 2000; Llave et al., 2006; Incarbona et al., 2011), it is likely that the freshwater budget of individual sub basins (or combinations thereof) did change sign. At present, marginal basins have a freshwater budget already close to zero (Zervakis et al., 2004; Raicich, 1996). Note that when the freshwater budget briefly changes sign, the direction of the intermediate water flow at the strait is not directly affected, since the intermediate current only changes direction when the density difference changes sign. Moreover, estimates of the increase of Nile discharge at sapropel times indicate that the freshwater budget of the Eastern Mediterranean may have changed sign (Amies et al., 2019). Aiming to study the effect of the freshwater budget of parts of the basin changing sign, we chose a forcing that emphasizes this behaviour. We present two model runs, for the first run the forcing is chosen to reflect the conditions during sapropel S5. Amies et al. (2019) found that the peak Nile outflow was eight times larger than present. We apply the same methodology to the Holocene sapropel, S1. Vadsaria et al. (2019) estimated that the Nile outflow during S1 was five times the present value, using a regional ocean–atmosphere coupled model, which includes simulations of ϵNd distribution. While the Nile flows into the open basin, our model is also very sensitive to the maximum river discharge into the marginal boxes for which, unfortunately, quantitative reconstructions are lacking. Therefore, besides a less augmented river discharge into the open basin, we use the same settings as for the S5 run to study S1.

The temperature, salinity and density of each box are calculated for each time step based on the exchange of properties with the surrounding boxes. We post-processed the resulting box temperatures with a so-called wavelet analysis, using the Matlab code from Torrence and Compo (1998), as described in Dirksen et al. (2019).

3. Results

The model results are shown in Figs. 2 and 4. For the first run the forcing is chosen to reflect conditions during sapropel S5, while the second run uses a lower river outflow in the open basin to reflect S1 reconstructions.

Three main intervals, delineated by vertical lines, can be identified in the S5 run: during the first 6.8 *kyr* the responds linearly to the forcing.

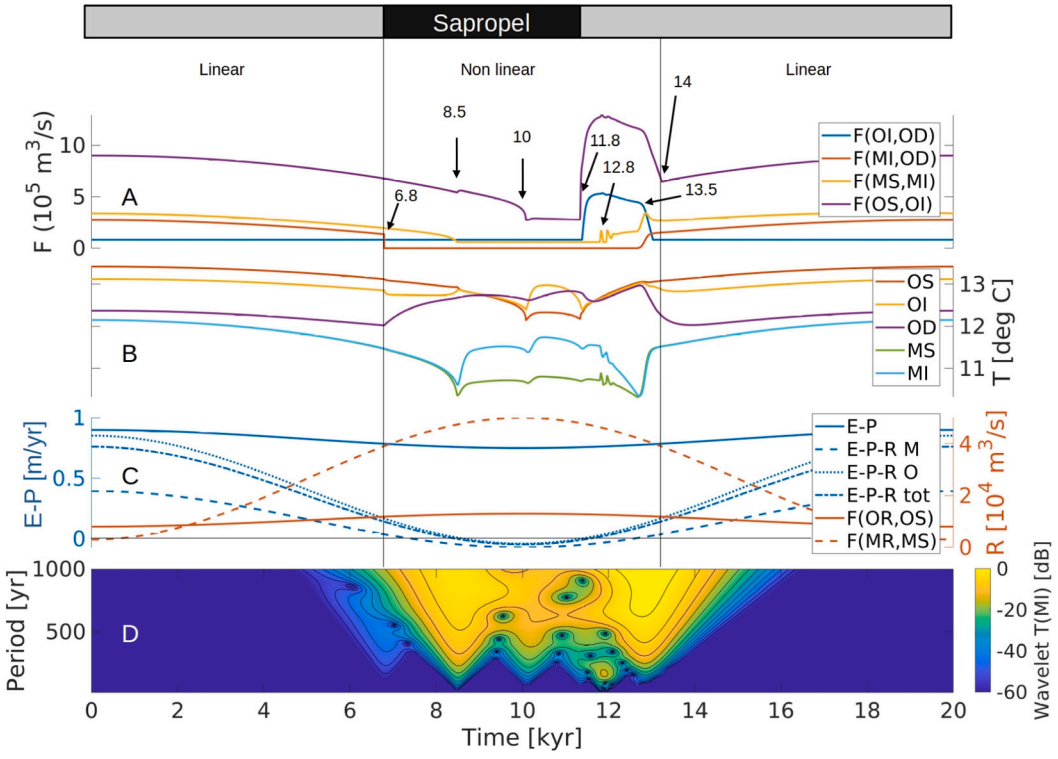

Fig. 2. An overview of the model run. Time runs from left to right. **A:** all downward fluxes F in [m^3/s], between the box combinations (OI,OD), (MI,OD), (MS,MI) and (OS,OI). The horizontal axis represents the time after spin up. The vertical lines indicate the transition from a linear to a non-linear regime where abrupt changes in fluxes occur. The arrows indicate the transitions in circulation and water properties indicated by the time in [*kyr*]. The sapropel interval, indicated by the black bar, is defined as the situation in which the only exchange with the open deep water box is background mixing with the overlying box. It starts at 6.8 *kyr*, when the deep water formation from the margins stops, and ends at 11.8 *kyr*, when deep convection in the open basin starts. **B:** the temperatures of the corresponding boxes. Note that when fluxes abruptly change, the temperature also changes significantly. **C:** the model forcing and freshwater budget for the various boxes. The horizontal black line indicates a freshwater budget of 0. The left vertical axis represents the net evaporation of the entire basin (*E*-P), and the freshwater budgets of each sub basins and the whole basin are shown in blue, in *m/s*. The right vertical axis represents the river outflow of each sub basin is shown in red, in 10^4 m^3/s. **D:** the wavelet analysis of the temperature of box MI. The colours indicate the spectral power of the frequencies through time in dB, yellow represents high power and blue low power. Wavelet analysis is a convenient tool to determine the periodicities of this time domain signal. Peaks and notches are found during the non-linear regime, typically in the range of 100–1000 years, much faster than the forcing. (For interpretation of the references to colour in this figure legend, the reader is referred to the web version of this article.)

The second interval, from 6.8 to 14 *kyr*, in which sapropel formation is predicted, is characterized by strong non-linear behaviour. Finally, in the third interval, from 14 *kyr* onward, the system returns to the initial state. Figs. 2A-C show the vertical fluxes, box temperatures and model forcing respectively, while Fig. 2D shows the wavelet transform of the marginal intermediate water temperature. Note that the non-linear interval shows multi-centennial variability. In this section we provide a detailed description of these results.

Previously we found that a change in sign of the freshwater budget of parts of the basin causes non-linearities, including a sudden termination of sapropel conditions (Dirksen and Meijer, 2020). As explained, we again assume a positive freshwater budget for part of the cycle, see Fig. 2C.

When fluxes stop or reverse direction, the equilibrium state changes abruptly. Consequently, the model relaxes towards this new equilibrium. This non-linear behaviour is unrelated to the forcing frequency. Generally, this process is expressed as a 'discontinuity' in the first derivative of, most prominently, temperature or volume flux, i.e. an abrupt change. The salinity and consequently density are much more directly affected by the forcing and therefore primarily show linear behaviour.

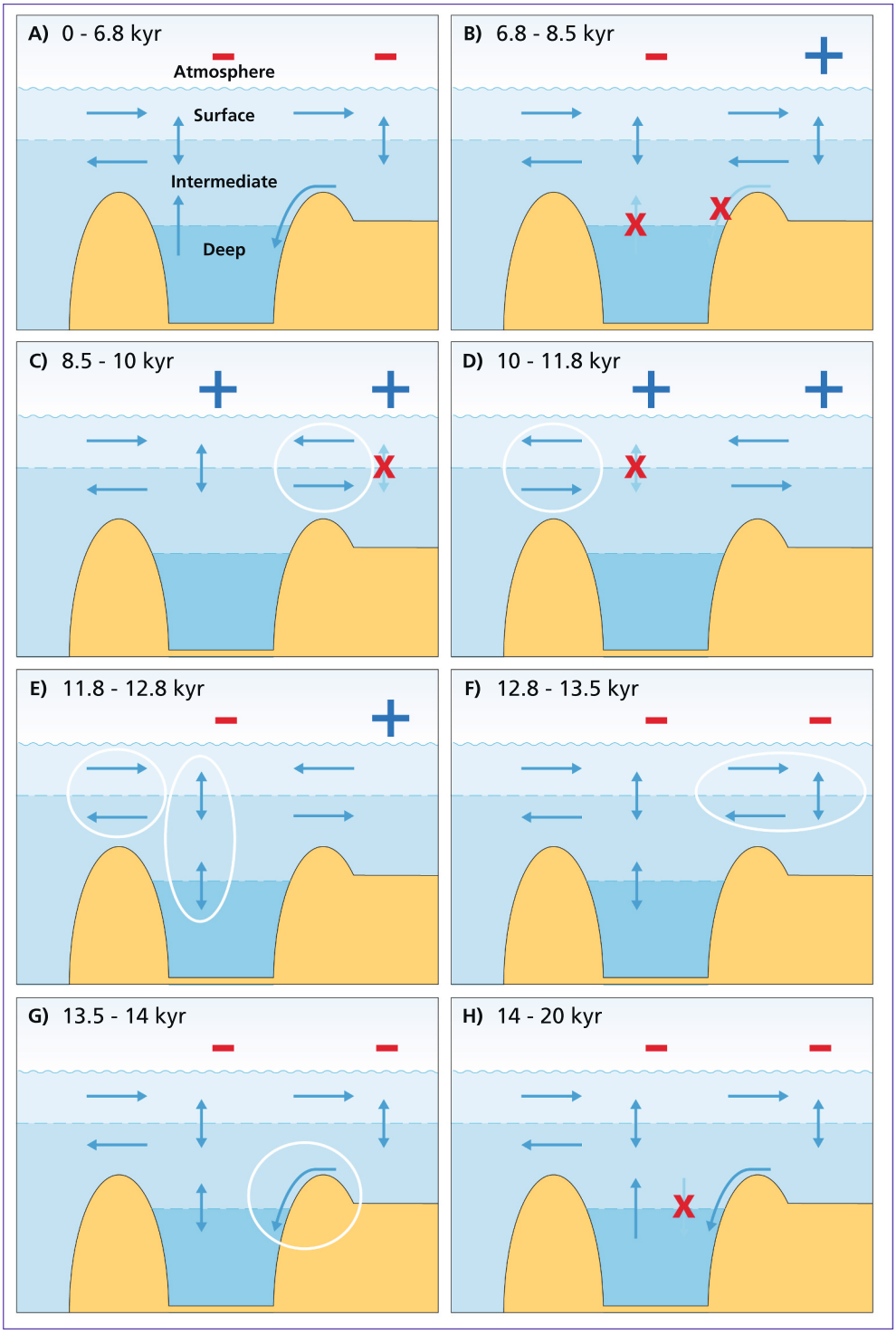

Fig. 3. A schematic overview of the various states of the circulation according to the model run. Only the most important fluxes are shown. The signs in the atmosphere indicate the freshwater budget of the basins. A red minus indicates a negative freshwater budget, while a blue plus indicates a positive freshwater budget. The panels refer to the time intervals delineated by the arrows in Fig. 2, i.e. 0 – 6.8 *kyr*, 6.8 – 8.5 *kyr*, 14 – 20 *kyr*. The first panel is equal to the last panel, completing the cycle. New fluxes, or fluxes that changed direction are encircled, while vanishing fluxes are crossed out. (For interpretation of the references to colour in this figure legend, the reader is referred to the web version of this article.)

We describe the various states of the circulation found in the model run in Fig. 2. A schematic overview of the circulation pattern of each state is given in Fig. 3. At the start of the run, from 0 to 6.8 *kyr*, the circulation is in a linear regime, which is sketched in Fig. 3A. Water flows into the open Mediterranean surface box to compensate for the density driven flux towards the Atlantic box and the fresh water deficit of both the marginal and open surface box. In the open surface box there is convection with the underlying intermediate box, a flux to the same intermediate box to compensate for the density driven outflow to the Atlantic box (this and other compensating vertical fluxes in addition to convection are not shown separately in Fig. 3) and a compensating flux towards the marginal surface box. In the marginal surface box there is convection with the marginal intermediate box and a compensating flux towards the intermediate box to allow for conservation of volume. In the marginal intermediate box there is density driven flux towards the open boxes, which sinks to the open deep box. From the open deep box there is a flux to compensate for this deep water formation towards the open intermediate box. In the open intermediate box there is in turn a flux of the same magnitude towards the open surface box to compensate for the water coming from the deep box.

The system transitions to a non-linear regime at 6.8 *kyr*, shown in Fig. 3B. The flux from the marginal intermediate box to the open deep box stops (Fig. 2A) because the density of the marginal intermediate box no longer exceeds the density of the open deep box, due to the decreased net evaporation and increased river outflow (Fig. 2C). Since the deep water box is only exchanging properties with the overlying intermediate box, its temperature starts to relax towards the temperature of the intermediate open box (Fig. 2B). The time scale depends on the volume of the deep box and magnitude of mixing. The wavelet analysis in Fig. 2D shows that the initial response is best described as a broad spectrum with emphasis on longer periods, with sharp notches, confined both in frequency and time, surrounding the peaks.

Next, at 8.5 *kyr*, the convection in the marginal boxes stops (Fig. 2A and Fig. 3C). This logically mainly affects the properties of the marginal boxes. The temperature of the intermediate water relaxes to a value closer to that of the open intermediate box because it has less interaction with the overlying box and water now flows into it from the open intermediate box. Furthermore, the salinity of the marginal surface box quickly decreases due to the increased river outflow and decreased exchange with the surrounding boxes with higher salinity.

The next major transition occurs at 10 *kyr* when the intermediate water exchange with the Atlantic reverses. As was the case for the marginal basin and illustrating what was pointed out in the Methods section, the reversal of exchange occurs well after the change in sign of the water budget: 1.6 *kyrs* later. Also at 10 *kyr*, the convection between the surface and intermediate water in the open basin stops (Fig. 3D), i.e. complete stagnation occurs. The lack of exchange between the surface and intermediate water, besides background mixing, causes the open intermediate water conditions to relax to values closer to the Atlantic water, i.e. the temperature increases. Similarly, the marginal intermediate box now mainly exchanges water with the open intermediate box, causing the temperature to increase, albeit to a lesser extent. The deep water also relaxes to the open intermediate water conditions. The larger volume of the deep box and limited exchange result in a much slower relaxation. The surface boxes have a strong exchange with the atmosphere relative to the background mixing with the intermediate water boxes, resulting in a small temperature change.

After this point the freshwater budget starts to decrease again (*E*-P-R moving towards more positive values in Fig. 2C). As a result convection occurs in all boxes of the open basin (Fig. 3E). This abruptly ends the interval with minimal deep water ventilation. Although the deep water is now ventilated again, the circulation has not yet reached the equivalent of the present-day state. Two brief intervals of convection occur in the marginal basin at 11.8 *kyr* when buoyancy loss in the surface box occurs again (Fig. 3F).

Next at 12.8 *kyr*, there is a brief interval with deep vertical convection, convection at the margins and deep water formation (Fig. 3H). Finally, the deep convection stops and the equivalent of the present day circulation is reached at 13.5 *kyr* (Fig. 3H). The deep water temperature only reaches dynamic equilibrium at roughly 14 *kyr*. Note that the open deep water box responds much slower than the other boxes at all transitions because it has a much larger volume.

The S1 run, shown in Fig. 4, shows very similar behaviour to the S5 run. With five times the present Nile outflow during the precession minimum, our model reaches a stagnation of deep water formation and convection in the marginal boxes and a reduction in intermediate convection in the open basin, i.e. the regime C in Fig. 3. In contrast to the S5 model results, the density driven intermediate water exchange with the Atlantic box does not reverse and the intermediate convection never fully stops. Instead, the model directly transitions from regime C to regime E, although with a slower onset of convection. Otherwise the behaviour of the model is the same as in the S5 run.

4. Discussion and conclusion

The precessional forcing of the freshwater budget can cause abrupt changes in the circulation. The model shows how, in response to this, the different (parts of) basins relax towards a new equilibrium state with a time scale $\tau \sim V/F$, with the volume V and through flow F. Although precession is a relatively slow process with a period of 20 *kyr*, a change in circulation can introduce much faster variability in the order of $\tau \sim 0.1 - 1$ *kyr*. For example, for the marginal intermediate box, with a volume of $2.25 \cdot 10^{14}\ m^3$ and a typical flux magnitude of $2 \cdot 10^5\ m^3/s$, we find a time scale of ~70 *yrs*. When the magnitude of the fluxes increases, the time scale decreases. For example, towards the end of the sapropel interval the fluxes slow down and as a consequence we see the peaks and notches shift towards longer periods in the wavelet transform (Fig. 2D). Note that frequencies of the peaks and notches observed in Fig. 2D are indeed in the same order of magnitude as the time scales found using the formula above. When the equilibrium state of a set of coupled boxes changes, those boxes will only reach their equilibrium when the box with the longest time scale has done so. The boxes with shorter time scales will initially approach their equilibrium state relatively fast (following their own time scale), until they are in dynamic equilibrium with a box with a longer time scale. From that point onwards the fast box will approach the equilibrium with the time scale of the slower box. Consequently, we expect to find the time scales related to slower boxes in the signals of faster boxes, given that they are coupled. The wavelet analysis of the intermediate water temperature (Fig. 2) indeed also shows periodicities that are in the order of 800 *yrs*, which, using the formula above, is the time scale of the open deep water box in the relevant interval.

Given the importance of volume for the behaviour here emphasized, to what extent are our findings dependent on the representation with boxes of fixed dimensions? Note that the two sets of dynamic boxes in the model (the open basin and the marginal basin) represent basins in the Mediterranean Sea. Since the volume of these basins is constant on orbital time scales, this division is justified. The potential absence of, for example, a separate open intermediate water mass during part of the precession cycle, e.g. the linear interval in Fig. 2, is realistically captured by convection in the model, which effectively homogenises layers. At present, the surface and intermediate water are also mixed during winter (Schroeder et al., 2012). When, during the remainder of the cycle, the interfaces between the water masses were fixed, but at different depth than here assumed, or varied slowly around an average depth, we expect our time scales to still be in the correct order of magnitude. The same is likely true when, in reality, different water masses existed side by side at the same depth. We therefore conclude that the assumption of constant box volumes is valid. While we show a single model result to highlight the non linear response, this behaviour generally occurs when the freshwater budgets briefly become positive. We therefore conclude that the model results are robust.

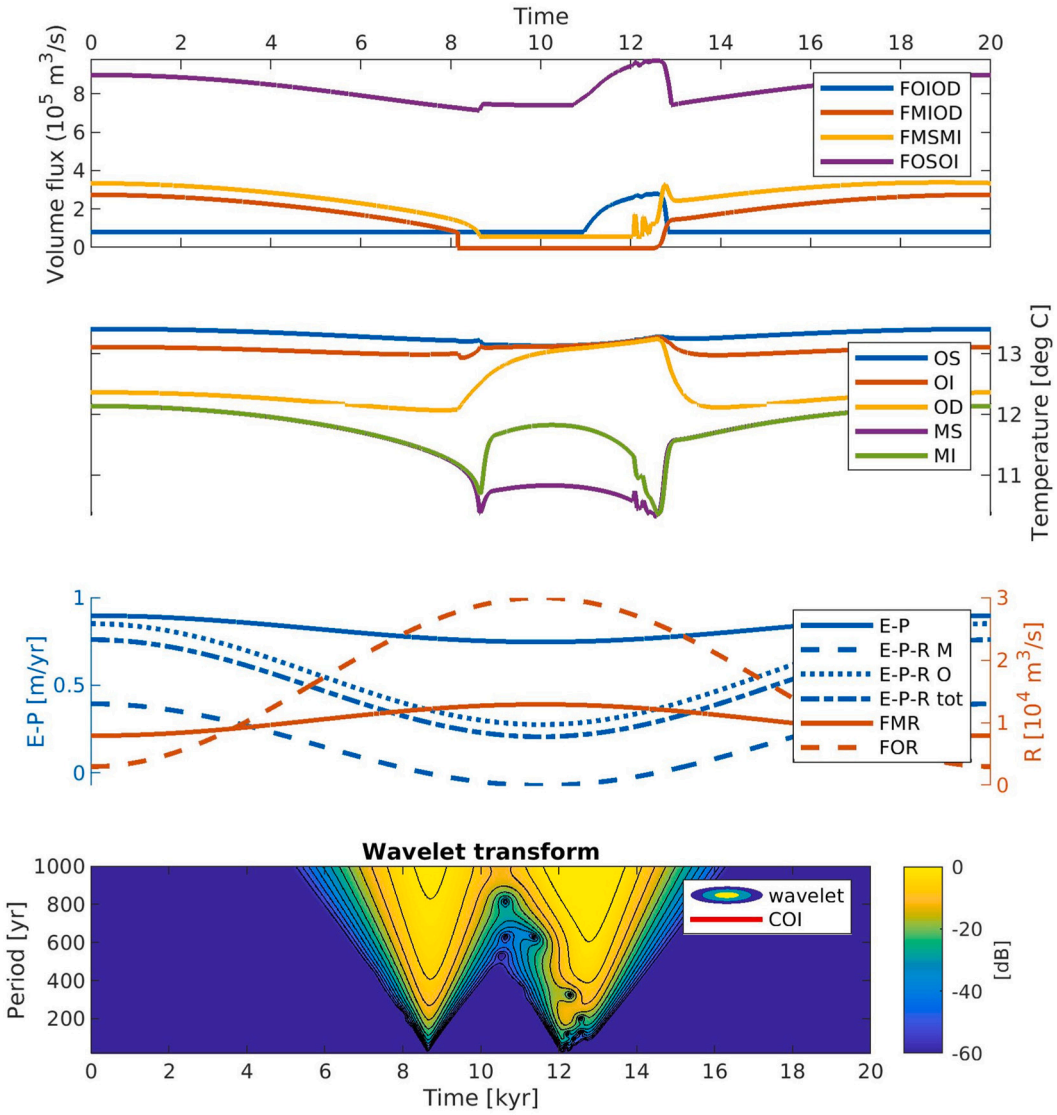

Fig. 4. An overview of the S1 model run. Time runs from left to right. **A:** all downward fluxes F in [m^3/s], between the box combinations (OI,OD), (MI,OD), (MS,MI) and (OS,OI). The horizontal axis represents the time after spin up. The vertical dashed lines indicate the transition from a linear to a non-linear regime where abrupt changes in fluxes occur. The arrows indicate the transitions in circulation and water properties indicated by the time in [*kyr*]. The sapropel interval, indicated by the black bar, is defined as the situation in which the only exchange with the open deep water box is background mixing with the overlying box. It starts at 6.8 *kyr*, when the deep water formation from the margins stops, and ends at 11.8 *kyr*, when deep convection in the open basin starts. **B:** the temperatures of the corresponding boxes. Note that when fluxes abruptly change, the temperature also changes significantly. **C:** the model forcing and freshwater budget for the various boxes. The left vertical axis represents the net evaporation of the entire basin (E-P), and the freshwater budgets of each sub basins and the whole basin are shown in blue, in *m/s*. The right vertical axis represents the river outflow of each sub basin is shown in red, in 10^4 m^3/s. **D:** the wavelet analysis of the temperature of box MI. The colours indicate the spectral power of the frequencies through time in dB, yellow represents high power and blue low power. Wavelet analysis is a convenient tool to determine the periodicities of this time domain signal. Peaks and notches are found during the non-linear regime, typically in the range of 100–1000 years, much faster than the forcing. (For interpretation of the references to colour in this figure legend, the reader is referred to the web version of this article.)

We compare our results to XRF data of sapropel S5 (128 − 121 *kyr*) in several sediment cores: 64PE406-E1 and ODP967 (Rodríguez-Sanz et al., 2017) in the Levantine basin and LC21 (Grant et al., 2016) in the Aegean Sea (Fig. 5). Barium (Ba) and the Barium/Titanium (Ba/Ti) ratio are proxies for productivity (e.g. Bishop, 1988; Dymond et al., 1992). The Ba/Ti records of S5 in core 64PE406-E1 and ODP967 are similar. They both show a gradual increase starting at 128 *kyr* and a sudden termination at 122 *kyr*. The Ba record of LC21 shows a large peak at the start of the sapropel, the difference compared to 64PE406-E1 and ODP967 may be explained by its location; it seems likely that productivity close to the Nile (64PE406-E1 and ODP967) was not the same as in the Aegean Sea (LC21).

These proxies show high-frequency variability in the sapropel interval in cores 64PE406-E1 and LC21 (Fig. 5). Proxies for bottom water anoxia (Mo/Ti Ziegler et al., 2008) and marine organic carbon (Br/Ti, e.g. Scott and Lyons, 2012; Tribovillard et al., 2006) in core 64PE406-E1 show very similar high-frequency variability (Dirksen et al., 2019). The proxies of these properties correlate with each other on even the shortest time scales (see the Monte-Carlo analysis in Dirksen et al., 2019). This implies that the Barium (productivity) variability also correlates with anoxia. The increased productivity is likely caused by increased Nile outflow, since the river water provides nutrients. The extra fresh water influx is also hypothesized to cause a stratified water column (Rossignol-Strick, 1985; Rohling et al., 2015). In the model, stratification occurs when the vertical fluxes (Fig. 5) are minimal, as a result of increased river outflow and decreased evaporation. The vertical

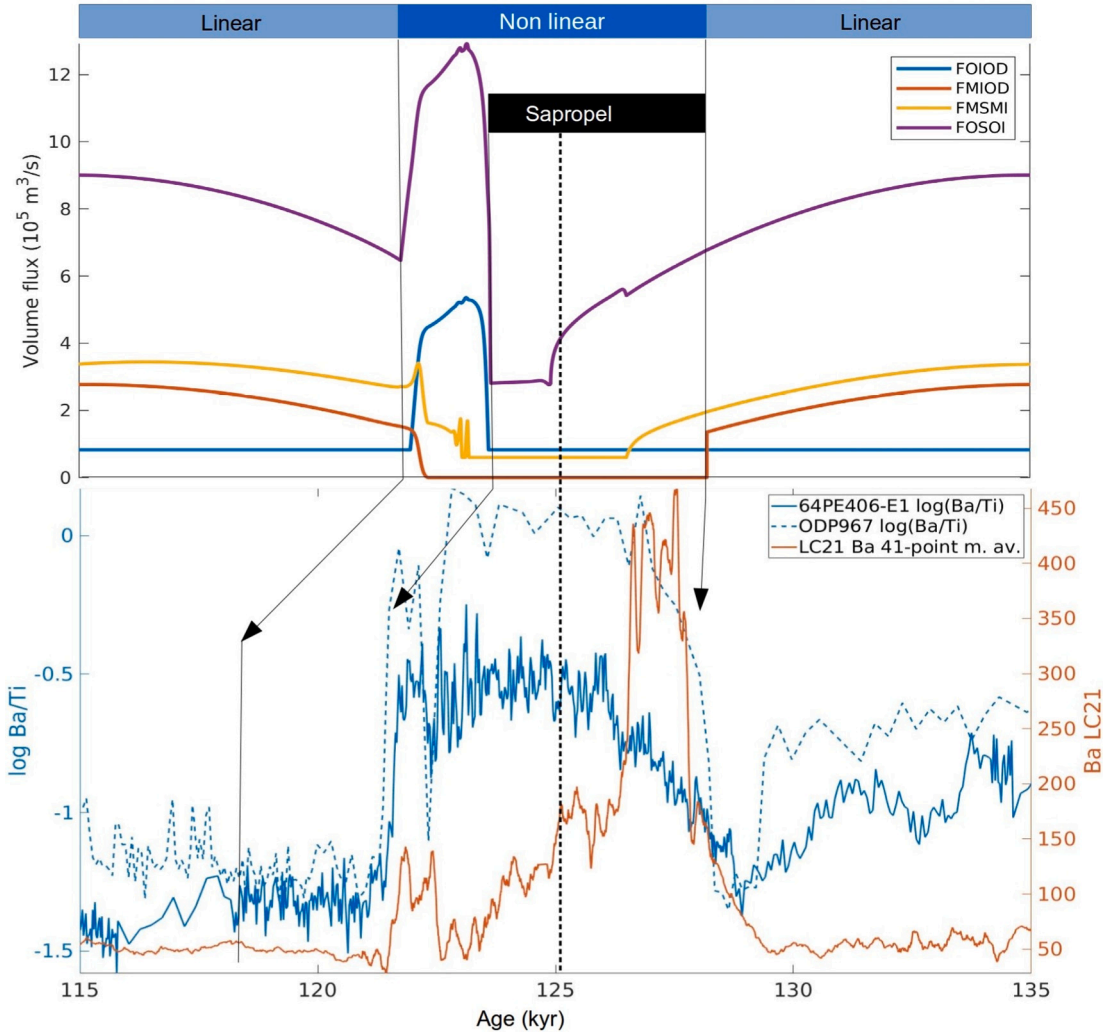

Fig. 5. The vertical fluxes of the model run (top panel) are compared with Ba/Ti XRF data from core 64PE406-E1 and ODP967, as well as Ba data from core LC21 (bottom panel). The time axis comprises a single precession cycle and runs from right to left. The vertical dashed line at 125 ka represents the approximate sapropel midpoint in the core data and the maximum of the river outflow and minimum net evaporation in the model. The arrows indicate transitions found in both the core data and the model run.

deep water fluxes in the model, FMIOD and FOIOD, are of particular interest, since the sediment cores are taken in deep parts of the basin and the sapropels in these cores therefore formed in the deep water.

The model predicts sudden changes in circulation, which causes the water properties to decay towards the new equilibrium. Such transitions would likely also affect productivity, since different water masses have different properties and nutrient concentrations. A sudden change in the equilibrium state is therefore expected to cause a similar decay towards a new equilibrium state in the proxies. Our model predicts such sudden changes and may therefore offer an alternative explanation for variability hitherto ascribed to high-frequency forcing (Dirksen et al., 2019).

Sapropel S5 is interrupted in core ODP967 (Rodríguez-Sanz et al., 2017) at 122 *kyr*, just before the end of the sapropel. The interruption coincides with an increase in productivity at LC21. This could be explained by convection or deep water formation in the Levantine basin (e.g. the regime in panel E in Fig. 3), supplying nutrients to the surface that accumulated during the stratified phase. The model does not predict an interruption, this is likely the result of the simplified forcing. Note that Dirksen et al. (2019) did not find an interruption in S5 in core 64PE406-E1. In our model we find that the stratification, when all downward fluxes are minimal, becomes unstable towards the end of the sapropel, at 11.8 *kyr* in Fig. 2A, corresponding to the transition from panel D to E in Fig. 3. After the interruption in the cores, sapropel formation briefly resumes, followed by a sudden termination at all core sites. This could either imply a sudden transition to the present day circulation, or a transition to a state where deep convection occurs in the Levantine basin and one or both marginal basins similar to regimes E, F or G in Fig. 3. The latter implies that while the sapropel is terminated, the circulation will still have to change to reach the linear state, which would introduce multi centennial scale variability in the interval directly after the sapropel. This would correspond with the non-linear interval directly after the sapropel in Fig. 5 between of 11 to 13 *kyr* in Fig. 2A and panels E,F and G in Fig. 3. Here the model indeed shows a different circulation than the present state: there is strong convection in all boxes and no deep water formation from the margins. The corresponding interval in the cores is bioturbated (see Fig. 4A in Dirksen et al., 2019), this bioturbation effectively acts as a low pass filter, meaning that the relevant variability may still be detectable. Furthermore, Dirksen et al. (2019) has shown that burn down did not occur (since there was no Mn/Ti peak after the sapropel) and as indicated by the results shown in Dirksen and Meijer (2020), directly resuming the normal circulation would likely not give a fast enough transition to prevent burn down. Note that the model forcing is a sine wave, while the actual monsoon intensity deviates. Nevertheless, the start of the the sapropel is correctly predicted, while the sapropel duration is underestimated, indicating that the actual forcing is not harmonic.

Next we compare frequency components and trends in the model with those found in core 64PE406-E1. We find that both show slowly varying frequencies in the order of 100–1000 years. The peaks in the wavelet transform of the core data in Dirksen et al. (2019) show an acceleration, i.e. longer periods, towards the end of the sapropel, similar to what we find in the model (Fig. 2D). In Dirksen et al. (2019) the modulation of the high-frequency components was interpreted as a the sedimentation rate variability. Here we propose an alternative mechanism. The time scale τ of this variability depends on the magnitude of the fluxes, as discussed above. Since the Nile outflow is expected to affect the magnitude of the fluxes, it should also modulate the high-frequency components. The model predicts that the main frequencies vary in time. Note that this hypothesis and the mechanism presented in Dirksen et al. (2019) are not mutually exclusive. The Nile flood record is known to correlate with Holocene solar variability (Ruzmaikin et al., 2006), so it seems likely that the discharge also showed this variability during the deposition of sapropel S5. In that case the Nile outflow would modulate the flux magnitudes directly, which would in turn modulate the time scale of any transitions. A modulation of the sedimentation rate would have had the same effect on the record, so it is possible that both of these mechanisms occurred simultaneously. With a sine wave forcing, our model captures the timing, termination and a significant part of the high frequency variability reasonably well. However, the characteristic laminations found in the sapropel in sediment cores are not reproduced by the model.

S1 has been studied extensively in sediment cores and with models. The rapid termination of the stratified state in our model due to deep convection in both presented runs is in agreement with the basin-wide, deep-water renewal found at the end of S1 formation by Wu et al. (2019). The formation of sapropel S1 may have been influenced by changes in sea level variations Cornuault et al. (2018). However, the ventilation in our model is not very sensitive to realistic changes in strait efficiency, i.e. the primary effect of sea level change. Furthermore, Vadsaria et al. (2019) indicate that the observed behaviour can largely be explained by monsoon variability.

We conclude that high-frequency variability in the Mediterranean Sea may not only result from high-frequency forcing, but also from non-linear internal variability. Specifically, abrupt changes in circulation cause the various parts of the basin to relax towards a new equilibrium state, the time scale of this relaxation depends on the volume of the water mass and the magnitude of the circulation. The time scales found in our model are in agreement with those found in sediment cores. We find that our model captures the overall behaviour of both S1 and S5.

Data statement

The annotated model code is available at https://doi.org/10.17605/OSF.IO/PQ5MY. The *. *m* files will run in Matlab, but can be viewed in any text editor.

Declaration of Competing Interest

The authors declare that they have no known competing financial interests or personal relationships that could have appeared to influence the work reported in this paper.

Acknowledgements

This work was financially supported by The Netherlands Research Centre for Integrated Solid Earth Science (ISES 2017-UU-23). The authors would like to thank Ronja Ebner for her help with the formulas and many useful discussions. We thank Ton Markus for the graphical design of Fig. 3. We thank the editor (Shu Gao), reviewer Cecile L. Blanchet and an anonymous reviewer for their constructive and thoughtful comments.

Appendix A

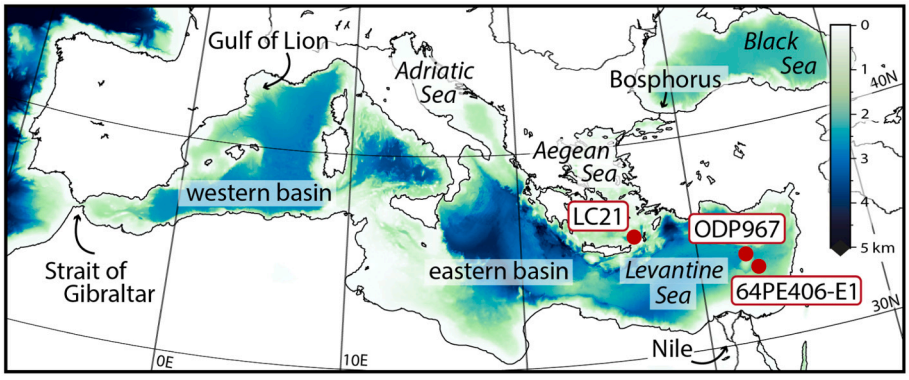

Fig. 6. A map of the Mediterranean Sea. The colour map indicates water depth in kilometres. The dots indicates the location of cores LC21, ODP967 and 64PE406-E1.

References

Amies, J., Rohling, E.J., Grant, K.M., 2019. Quantification of African Monsoon Runoff during last Interglacial Sapropel S5. Paleoceanogr. Paleoclimatol. 1–30.
Bibby, T., Putkonen, J., Morgan, D., Balco, G., Shuster, D.L., 2016. Million year old ice found under meter thick debris layer in Antarctica. Geophys. Res. Lett. 43 (13), 6995–7001.
Bishop, J.K., 1988. The barite-opal-organic carbon association in oceanic particulate matter. Nature 332 (6162), 341–343.
Cornuault, M., Tachikawa, K., Vidal, L., Guihou, A., Siani, G., Deschamps, P., Bassinot, F., Revel, M., 2018. Circulation changes in the eastern mediterranean sea over the past 23,000 years inferred from authigenic nd isotopic ratios. Paleoceanogr. Paleoclimatol. 33 (3), 264–280.
Dirksen, J.P., Meijer, P., 2020. The mechanism of sapropel formation in the Mediterranean Sea: insight from long-duration box model experiments. Clim. Past 16 (3), 933–952.
Dirksen, J.P., Hennekam, R., Geerken, E., Reichart, G.J., 2019. A novel approach using time-depth distortions to assess multicentennial variability in deep-sea oxygen deficiency in the eastern mediterranean sea during sapropel S5. Paleoceanogr. Paleoclimatol. 34 (5), 774–786.
Dymond, J., Suess, E., Lyle, M., 1992. Abstract. We used sediment traps to define the higher barium contents in the intermediate and combined our particle flux data with existing water linkages to ocean productivity and the degree of. Paleoceanography 7 (2), 163–181.
Grant, K.M., Grimm, R., Mikolajewicz, U., Marino, G., Ziegler, M., Rohling, E.J., 2016. The timing of Mediterranean sapropel deposition relative to insolation, sea-level and African monsoon changes. Quat. Sci. Rev. 140, 125–141.

Incarbona, A., Sprovieri, M., Lirer, F., Sprovieri, R., 2011. Surface and deep water conditions in the Sicily channel (Central Mediterranean) at the time of sapropel S5 deposition. Palaeogeogr. Palaeoclimatol. Palaeoecol. 306 (3–4), 243–248.
Llave, E., Schönfeld, J., Hernández-Molina, F.J., Mulder, T., Somoza, L., Díaz Del Río, V., Sánchez-Almazo, I., 2006. High-resolution stratigraphy of the Mediterranean outflow contourite system in the Gulf of Cadiz during the late Pleistocene: the impact of Heinrich events. Mar. Geol. 227 (3–4), 241–262.
Meijer, P., 2021. (paleo) oceanography of semi-enclosed seas with a focus on the mediterranean region; insights from basic theory. Earth Sci. Rev. 221, 103810.
Mercone, D., Thomson, J., Abu-Zied, R.H., Croudace, I.W., Rohling, E.J., 2001. High-resolution geochemical and micropalaeontological profiling of the most recent eastern Mediterranean sapropel. Mar. Geol. 177 (1–2), 25–44.
on Oceanographic Tables, J. P, 1986. Progress on Oceanographic Tables and Standards, 1983–1986: Work and Recommendations of the UNESCO/SCOR/ICES/IAPSO Joint Panel. Number 50 in UNESCO Tech. Pap. Mar. Unesco.
Raicich, F., 1996. On the fresh water balance of the Adriatic Sea. J. Mar. Syst. 9 (3–4), 305–319.
Rodríguez-Sanz, L., Bernasconi, S.M., Marino, G., Heslop, D., Mueller, I.A., Fernandez, A., Grant, K.M., Rohling, E.J., 2017. Penultimate deglacial warming across the mediterranean sea revealed by clumped isotopes in foraminifera. Sci. Rep. 7 (1), 1–11.
Rogerson, M., Rohling, E.J., Weaver, P.P., Murray, J.W., 2005. Glacial to interglacial changes in the settling depth of the Mediterranean Outflow plume. Paleoceanography 20 (3), 1–12.
Rohling, E.J., Marino, G., Grant, K.M., 2015. Mediterranean climate and oceanography, and the periodic development of anoxic events (sapropels). Earth Sci. Rev. 143, 62–97.
Rossignol-Strick, M., 1985. Mediterranean Quaternary sapropels, an immediate response of the African monsoon to variation of insolation. Palaeogeogr. Palaeoclimatol. Palaeoecol. 49 (3–4), 237–263.
Ruzmaikin, A., Feynman, J., Yung, Y.L., 2006. Is solar variability reflected in the Nile River? J. Geophys. Res.-Atmos. 111 (21), 1–8.
Sampieri, R.H., 2002. Climate Development and History of the North Atlantic Realm. Springer, Berlin Heidelberg, Berlin, Heidelberg.
Schönfeld, J., 2002. A new benthic foraminiferal proxy for near-bottom current velocities in the Gulf of Cadiz, northeastern Atlantic Ocean. Deep-Sea Res. Part I: Oceanogr. Res. Papers 49 (10), 1853–1875.
Schönfeld, J., Zahn, R., 2000. Late Glacial to Holocene history of the Mediterranean outflow. Evidence from benthic foraminiferal assemblages and stable isotopes at the Portuguese margin. Palaeogeogr. Palaeoclimatol. Palaeoecol. 159 (1–2), 85–111.
Schroeder, K., Garcìa-Lafuente, J., Josey, S.A., Artale, V., Nardelli, B.B., Carrillo, A., Gačić, M., Gasparini, G.P., Herrmann, M., Lionello, P., Ludwig, W., Millot, C., Özsoy, E., Pisacane, G., Sánchez-Garrido, J.C., Sannino, G., Santoleri, R., Somot, S., Struglia, M., Stanev, E., Taupier-Letage, I., Tsimplis, M.N., Vargas-Yáñez, M., Zervakis, V., Zodiatis, G., 2012. Circulation of the Mediterranean Sea and its Variability. Elsevier.
Scott, C., Lyons, T.W., 2012. Contrasting molybdenum cycling and isotopic properties in euxinic versus non-euxinic sediments and sedimentary rocks: refining the paleoproxies. Chem. Geol. 324-325, 19–27.
Sierro, F.J., Hodell, D.A., Andersen, N., Azibeiro, L.A., Jimenez-Espejo, F.J., Bahr, A., Flores, J.A., Ausin, B., Rogerson, M., Lozano-Luz, R., Lebreiro, S.M., Hernandez-Molina, F.J., 2020. Mediterranean Overflow over the last 250 kyr: freshwater forcing from the tropics to the Ice Sheets. Paleoceanogr. Paleoclimatol. 35 (9), 1–31.
Song, X., Yu, L., 2017. Air-sea heat flux climatologies in the Mediterranean Sea: Surface energy balance and its consistency with ocean heat storage. J. Geophys. Res. Oceans 122, 4068–4087.
Starr, A., Hall, I., Barker, S., Rackow, T., Zhang, X., Hemming, S., van der Lubbe, H., Knorr, G., Berke, M., Bigg, G., Cartagena, A., Jiménez-Espejo, F., Gong, X., Gruetzner, J., Lathika, N., LeVay, L., Robinson, R., Ziegler, M., 2020. Antarctic icebergs reorganise ocean circulation during pleistocene glacials. Nature 589 (January).
Timmermann, A., Gildor, H., Schulz, M., Tziperman, E., 2003. Coherent resonant millennial-scale climate oscillations triggered by massive meltwater pulses. J. Clim. 16 (15), 2569–2585.
Torrence, C., Compo, G.P., 1998. A Practical Guide to Wavelet Analysis. Bull. Am. Meteorol. Soc. 79 (1), 61–78.
Tribovillard, N., Algeo, T.J., Lyons, T., Riboulleau, A., 2006. Trace metals as paleoredox and paleoproductivity proxies: an update. Chem. Geol. 232 (1–2), 12–32.
Vadsaria, T., Ramstein, G., Dutay, J.-C., Li, L., Ayache, M., Richon, C., 2019. Simulating the occurrence of the last sapropel event (s1): Mediterranean basin ocean dynamics simulations using nd isotopic composition modeling. Paleoceanogr. Paleoclimatol. 34 (2), 237–251.
Wu, J., Pahnke, K., Böning, P., Wu, L., Michard, A., de Lange, G.J., 2019. Divergent mediterranean seawater circulation during holocene sapropel formation–reconstructed using nd isotopes in fish debris and foraminifera. Earth Planet. Sci. Lett. 511, 141–153.
Zahn, R., Sarnthein, M., Erlenkeuser, H., 1987. Benthic isotope evidence for changes of the Mediterranean outflow during the late Quaternary, 2 (6), 543–559.
Zervakis, V., Georgopoulos, D., Karageorgis, A.P., Theocharis, A., 2004. On the response of the Aegean Sea to climatic variability: a review. Int. J. Climatol. 24 (14), 1845–1858.
Ziegler, M., Jilbert, T., De Lange, G.J., Lourens, L.J., Reichart, G.J., 2008. Bromine counts from XRF scanning as an estimate of the marine organic carbon content of sediment cores. Geochem. Geophys. Geosyst. 9 (5), 1–6.